Video Article

Concurrent Quantitative Conductivity and Mechanical Properties Measurements of Organic Photovoltaic Materials using AFM

Maxim P. Nikiforov[1], Seth B. Darling[1,2]

[1]Center for Nanoscale Materials, Argonne National Laboratory

[2]Institute for Molecular Engineering, University of Chicago

Correspondence to: Maxim P. Nikiforov at maximnik@anl.gov

URL: http://www.jove.com/video/50293
DOI: doi:10.3791/50293

Keywords: Materials Science, Issue 71, Nanotechnology, Mechanical Engineering, Electrical Engineering, Computer Science, Physics, electrical transport properties in solids, condensed matter physics, thin films (theory, deposition and growth), conductivity (solid state), AFM, atomic force microscopy, electrical properties, mechanical properties, organic photovoltaics, microengineering, photovoltaics

Date Published: 1/23/2013

Citation: Nikiforov, M.P., Darling, S.B. Concurrent Quantitative Conductivity and Mechanical Properties Measurements of Organic Photovoltaic Materials using AFM. *J. Vis. Exp.* (71), e50293, doi:10.3791/50293 (2013).

Abstract

Organic photovoltaic (OPV) materials are inherently inhomogeneous at the nanometer scale. Nanoscale inhomogeneity of OPV materials affects performance of photovoltaic devices. Thus, understanding of spatial variations in composition as well as electrical properties of OPV materials is of paramount importance for moving PV technology forward.[1,2] In this paper, we describe a protocol for quantitative measurements of electrical and mechanical properties of OPV materials with sub-100 nm resolution. Currently, materials properties measurements performed using commercially available AFM-based techniques (PeakForce, conductive AFM) generally provide only qualitative information. The values for resistance as well as Young's modulus measured using our method on the prototypical ITO/PEDOT:PSS/P3HT:PC_{61}BM system correspond well with literature data. The P3HT:PC_{61}BM blend separates onto PC_{61}BM-rich and P3HT-rich domains. Mechanical properties of PC_{61}BM-rich and P3HT-rich domains are different, which allows for domain attribution on the surface of the film. Importantly, combining mechanical and electrical data allows for correlation of the domain structure on the surface of the film with electrical properties variation measured through the thickness of the film.

Video Link

The video component of this article can be found at http://www.jove.com/video/50293/

Introduction

Recent breakthroughs in power conversion efficiency (PCE) of organic photovoltaic (OPV) cells (pushing 10% at the cell level)[3] in concert with compliance with high-throughput and low-cost manufacturing processes[4] have brought a spotlight onto OPV technology as a possible solution for the challenge of inexpensive manufacturing of large-area solar cells. OPV materials are inherently inhomogeneous at the nanometer scale. Nanoscale inhomogeneity of OPV materials and performance of photovoltaic devices are intimately connected. Thus, understanding inhomogeneity in composition as well as electrical properties of OPV materials is of paramount importance for moving OPV technology forward. Atomic force microscopy (AFM) has been developed as a tool for high-resolution measurements of surface topography since 1986.[5] Nowadays, techniques for materials properties (Young's modulus,[6-10] work function,[11] conductivity,[12] electromechanics,[13-15] etc.) measurements are attracting increasing attention. In the case of OPV materials, correlation of local phase composition and electrical properties holds promise for revealing better understanding of the inner workings of organic solar cells.[1, 16-17] AFM-based techniques are capable of high-resolution phase attribution[8] as well as electrical properties mapping in polymeric materials. Thus, in principle, correlation of polymer phase composition (through mechanical measurements)[18] and electrical properties is possible using AFM-based techniques. Many AFM-based techniques for measurements of mechanical and electrical properties of materials use the assumption of constant area of contact between the AFM probe and the surface. This assumption often fails, which results in strong correlation among surface topography and mechanical/electrical properties. Recently, a new AFM-based technique for high-throughput measurements of mechanical properties (PeakForce)[19] was introduced. PeakForce TUNA (variation of the PeakForce method) provides a platform for concurrent measurements of mechanical and electrical properties of the sample. However, the PeakForce TUNA method produces mechanical and electrical property maps, which usually are strongly correlated because of unaccounted variability of contact during measurements. In this paper, we present an experimental protocol for removing correlations associated with varying contact radius while maintaining accurate measurements of the mechanical and electrical properties using AFM. Implementation of the protocol results in quantitative measurements of materials' resistance and Young's Modulus.

Protocol

1. Signal Acquisition

a. Install sample (polymer solar cell without cathode (ITO/PEDOT:PSS/P3HT:$PC_{61}BM$)) into a commercial Multimode AFM (Veeco, Santa Barbara, CA) equipped with Nanoscope-V controller.
b. Install conductive AFM probe into Multimode AFM probe holder.
c. Create electrical connection between the AFM probe, sample and voltage source.
d. Route current amplifier output (current signal), Multimode AFM deflection output (force signal), Multimode AFM sample height output (distance signal) into a digital acquisition card (NI-PCI-6115 DAQ). The gain on Femto DLPCA-200 current amplifier is 1 nA/V at 50 kHz bandwidth.
e. Apply 6V bias between AFM probe and ITO electrode.
f. Run Multimode AFM in PeakForceTM mode collecting topography signal: peak force set point of 30 nN, a support oscillation amplitude of 300 nm, a support oscillation frequency of 2 kHz, a scan rate of 1 Hz, and a resolution of 512 by 512 pixels.
g. Collect signals listed in section d by LabView/MATLAB control concurrently with acquisition of topography signal (step e).

2. Data Analysis Step 1: Generation of Pull-off Force, Contact Stiffness, and Current Maps

a. Read time-stamped current, force and distance signals into MATLAB.
b. Create 2,000 force - distance, and force - current curves for the first scan line. Number of curves is a function of support oscillation frequency and scan rate.
c. From each force - distance curve, determine contact stiffness and pull-off-force during withdrawal of the AFM probe (**Figure 1**).
d. From each force - current curve, determine the average current while the AFM probe is in contact with the surface during withdraw (**Figure 1**).
e. Interpolate 2,000 equally spaced contact stiffness, pull-off-force, and current points by 512 points to match resolution of topography signal. The first scan line for contact stiffness, pull-off-force, and current maps is done.
f. Create contact stiffness, pull-off-force, and current maps by repeating steps b through e 512 times. Results are shown in **Figure 2**.

3. Data Analysis Step 2: Elimination of Contact-area Artifacts

a. Use equation (1) and (2) to obtain Young's Modulus ($E_{MATERIAL}$) and resistance (ρ) of the material at each point of the scan:[20]

$$E_{MATERIAL} = (0.2 \pm 0.1) \cdot w^{1/2} \cdot k^{3/2} / F_{ADH} \qquad (1)$$

$$\rho \cong (16 \pm 12) \frac{F_{ADH}^{4/3} V}{I L w^{2/3} k^{2/3}} \qquad (2)$$

using $F_{ADH} = F_{PULL}$ - 8 nN (adhesion due to water meniscus between the AFM and the surface),[20] contact stiffness (k), and current (I) maps; probing voltage (V), film thickness (L), and adhesion energy ($w = \gamma_{PROBE} + \gamma_{MATERIA}L - \gamma_{PROBE-MATERIAL}$, where γ_{PROBE} - surface energy of probe material, $\gamma_{MATERIAL}$ - surface energy of sample material, and $\gamma_{PROBE-MATERIAL}$ - interfacial energy of sample material and probe material).[20]

Representative Results

Young's modulus and resistivity maps (**Figure 3**) present typical results of the measurements described above. Mechanical and electrical properties of the ITO/PEDOT:PSS/P3HT:$PC_{61}BM$ stack were measured at negative (-10 V) and positive (+6 V) voltages applied to the AFM probe. Imaging artifacts, associated with electrostatic interaction between the AFM probe and the sample, are a common problem for quantitative measurements of functional properties using AFM. The similarity of Young's moduli magnitude measured at different voltages demonstrates robustness of the measurement protocol described above with respect to electrostatic artifacts. Often variations in chemical composition within a material are associated with the local changes in Young's modulus. The sample used in this study is a solar cell device without the top electrode. The top layer (P3HT:$PC_{61}BM$) in the stack is the solar cell active layer where conversion of light into electricity occurs. Solar cell performance strongly depends on the morphology and chemical composition of the active layer.

Contact stiffness and current measured using AFM are often correlated (**Figure 4**) because of the variations in contact area between the AFM probe and the surface. Such correlation often complicates quantitative determination of mechanical (Young's Modulus) and electrical (resistivity) properties of the material. The protocol, provided above, accounts for variations in contact area by direct measurements of the adhesion force between the AFM probe and the surface, which in turn allows for quantitative measurements of Young's modulus and resistivity. $PC_{61}BM$-rich domains are stiffer than polymer-rich ones. Failure to account for contact area variability leads to domain misrepresentation. For example, stiff $PC_{61}BM$-rich domain is visible on both contact stiffness and Young's modulus's line profiles (**Figure 4A**), while the other $PC_{61}BM$-rich domain (**Figure 4B**) appears only on Young's modulus map.

The method described above allows for attribution of chemical composition on the surface of the P3HT:$PC_{61}BM$ layer. Two types of domains with different Young's moduli are evident in **Figure 3(A)** and **3(B)**. Knowledge about chemical composition of the active layer and literature data on mechanical properties of P3HT[21-26] and $PC_{61}BM$[21] allows attribution of domains with Young's modulus around 0.01 GPa as P3HT-rich ones (appear blue on **Figure 3(A)** and **(B)**) and domains with Young's modulus around 0.1 GPa as $PC_{61}BM$-rich ones (appear dark red on **Figure 3(A)** and **(B)**).[27] Resistance maps (**Figure 3(C)** and **(D)**) provide information about electrical connectivity between the top surface of

the P3HT:PC_{61}BM layer and the ITO layer. In an operating solar cell, current travels from the bulk of the active layer toward current collectors (ITO and the electrode deposited on top of the P3HT:PC_{61}BM layer, respectively), thus, resistance maps are vital pieces of information that allow for correlation of chemical composition and performance of solar cells. **Figures 3(C) and 3(D)** show that resistance of P3HT-rich and PC_{61}BM-rich domains changes depending on the polarity of voltage applied to the AFM probe. P3HT-rich domains have lower resistance at positive voltage and higher resistance at negative voltage in comparison with PC_{61}BM-rich domains. Possible injection of holes from the high-work function Pt probe, relatively high hole conductivity of P3HT[28] and hole conductivity of PEDOT:PSS explain lower resistance of the P3HT-rich areas, as well as a higher barrier for electron injection and electron rejection properties of PEDOT:PSS were cited[27] as reasons for higher resistance of the PC_{61}BM-rich domains in comparison with P3HT-rich ones under positive bias of the AFM probe. At negative bias, resistance of P3HT-rich domains should increase and resistance of PC_{61}BM domains should decrease because of a decrease in hole injection efficiency of PEDOT:PSS[29] (resulting in decrease of electron rejection) and injection of electrons from the negatively biased Pt probe. Chemical attribution of domains based on mechanical properties measurements is valid only in proximity of the air-P3HT:PC_{61}BM interface, while resistance measurements provide information about current pathways through the thickness of the film. In this regard, mechanical and electrical measurements provide complimentary information about the sample. Variation in resistance within P3HT-rich and PC_{61}BM-rich surface domains reveals inhomogeneity of the domain structure throughout the active layer film thickness.

Summarizing, we described a protocol for quantitative measurements of Young's modulus and resistivity of soft materials by mitigating contact area uncertainty. Mechanical properties of PC_{61}BM-rich and P3HT-rich domains are different, which allow for domain attribution on the surface of the film. Combination of mechanical and electrical data allows for correlation of the domain structure on the surface of the film with electrical properties variation measured through the thickness of the film.

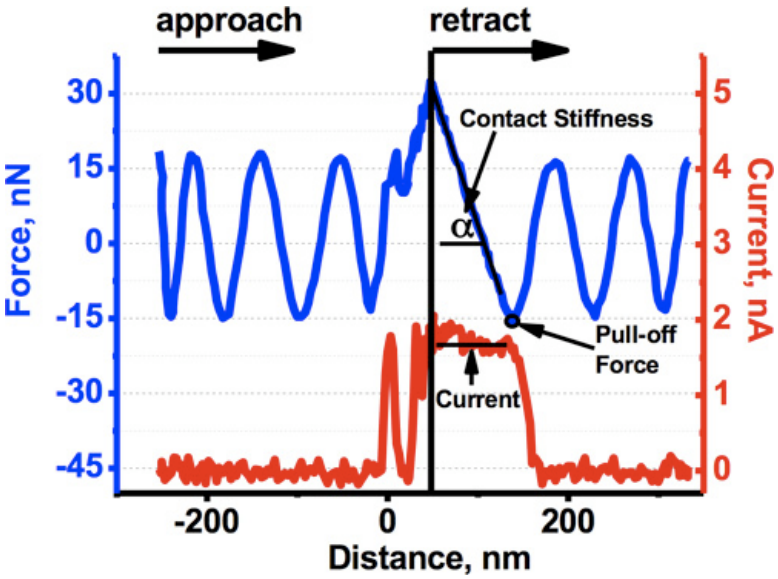

Figure 1. Typical force - distance (blue) and current - distance (red) curves taken on ITO/PEDOT:PSS/P3HT:PC_{61}BM with Pt probe.

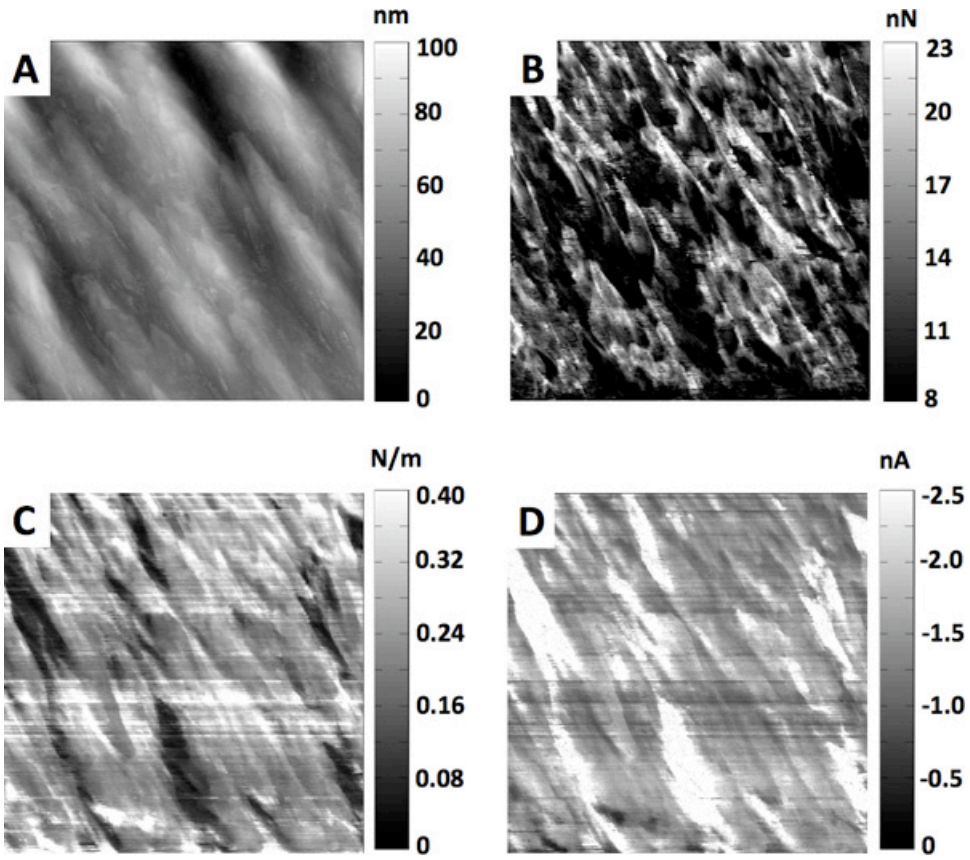

Figure 2. Spatially resolved measurements of topography (A), pull-off force (B), contact stiffness (C), and conductivity at -10 V (D) on an ITO/PEDOT:PSS/P3HT:PCBM sample. Image size is 10 µm x 10 µm.

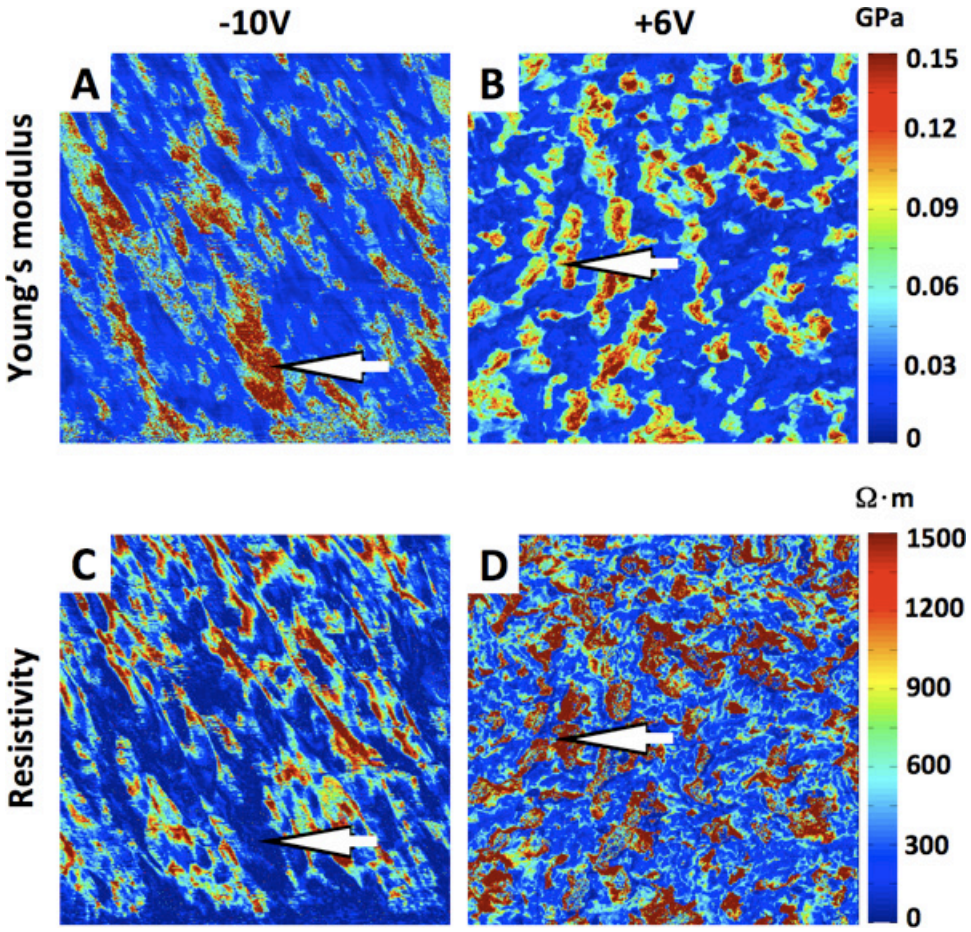

Figure 3. Spatially resolved variations of Young's Modulus (A, B) and resistivity (C, D) for two different locations on the surface measured at -10 V (A, C) and 6 V (B, D). Images (A) and (C) were calculated from the data presented in **Figure 2**. Image size is 10 µm x 10 µm. White arrows point toward $PC_{61}BM$-rich domains, which demonstrate resistivity switch as a function of voltage polarity (low resistivity at negative bias and high resistivity at positive bias). Black dotted line (A, C) indicates areas used for line profiles on **Figure 4**.

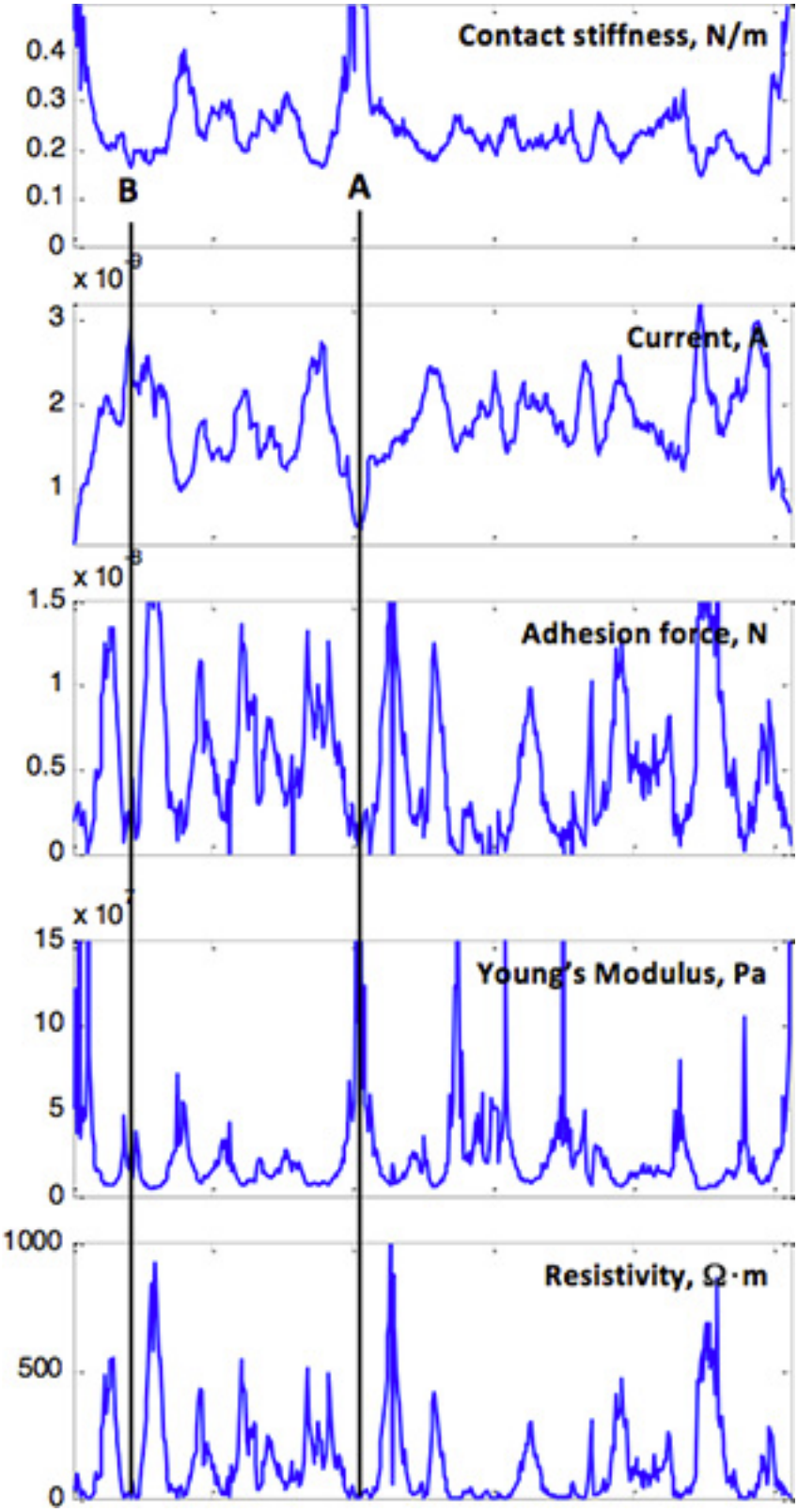

Figure 4. Line profiles from the areas indicated with black dotted lines on **Figures 2 and 3A, 3C**. Strong correlation between contact stiffness and current due to contact radius variability is apparent. Elimination of contact radius variations reveals stiff $PC_{61}BM$-rich domains, which are poorly visible otherwise (B). Click here to view larger figure.

Disclosures

No conflicts of interest declared.

Acknowledgements

MPN is grateful to the Director's Fellowship Program for financial support. MPN wants to thank Yu-Chih Tseng for help with development of the protocol for solar cell processing. This work was performed at the Center for Nanoscale Materials, a U.S. Department of Energy, Office of Science, Office of Basic Energy Sciences User Facility under Contract No. DE-AC02-06CH11357.

References

1. Chen, W., Nikiforov, M.P., & Darling, S.B. Morphology characterization in organic and hybrid solar cells. *Energy Environ. Sci.*, doi:10.1039/C2EE22056C (2012).
2. Dupont, S.R., Oliver, M., Krebs, F.C., & Dauskardt, R.H. Interlayer adhesion in roll-to-roll processed flexible inverted polymer solar cells. *Sol. Energy Mater. Sol. Cells.* **97**, 171-175 (2012).
3. Green, M.A., Emery, K., Hishikawa, Y., Warta, W., & Dunlop, E.D. Solar cell efficiency tables (version 39). *Progress in Photovoltaics.* **20** (1), 12-20 (2012).
4. Krebs, F.C., Gevorgyan, S.A., & Alstrup, J. A roll-to-roll process to flexible polymer solar cells: model studies, manufacture and operational stability studies. *Journal of Materials Chemistry.* **19** (30), 5442-5451 (2009).
5. Binnig, G., Quate, C.F., & Gerber, C. Atomic Force Microscope. *Physical Review Letters.* **56** (9), 930-933 (1986).
6. Hurley, D.C., Kopycinska-Muller, M., Kos, A.B., & Geiss, R.H. Nanoscale elastic-property measurements and mapping using atomic force acoustic microscopy methods. *Measurement Science & Technology.* **16** (11), 2167-2172 (2005).
7. Jesse, S., Nikiforov, M.P., Germinario, L.T., & Kalinin, S.V. Local thermomechanical characterization of phase transitions using band excitation atomic force acoustic microscopy with heated probe. *Applied Physics Letters.* **93** (7) (2008).
8. Nikiforov, M.P., Gam, S., Jesse, S., Composto, R.J., & Kalinin, S.V. Morphology Mapping of Phase-Separated Polymer Films Using Nanothermal Analysis. *Macromolecules.* **43** (16), 6724-6730 (2010).
9. Nikiforov, M.P., Jesse, S., Morozovska, A.N., Eliseev, E.A., Germinario, L.T., & Kalinin, S.V. Probing the temperature dependence of the mechanical properties of polymers at the nanoscale with band excitation thermal scanning probe microscopy. *Nanotechnology.* **20** (39) (2009).
10. Rabe, U., Amelio, S., Kopycinska, M., Hirsekorn, S., Kempf, M., Goken, M., & Arnold, W. Imaging and measurement of local mechanical material properties by atomic force acoustic microscopy. *Surface and Interface Analysis.* **33** (2), 65-70 (2002).
11. Nikiforov, M.P., Zerweck, U., Milde, P., Loppacher, C., Park, T.-H., Uyeda, H.T., Therien, M.J., Eng, L., & Bonnell, D. The effect of molecular orientation on the potential of porphyrin-metal contacts. *Nano Letters.* **8** (1), 110-113 (2008).
12. Nikiforov, M.N., Brukman, M.J., Bonnell, & D.A. High-resolution characterization of defects in oxide thin films. *Applied Physics Letters.* **93** (18), (2008).
13. Kalinin, S.V., Karapetian, E., & Kachanov, M. Nanoelectromechanics of piezoresponse force microscopy. *Physical Review B.* **70** (18), (2004).
14. Kolosov, O., Gruverman, A., Hatano, J., Takahashi, K., & Tokumoto, H. Nanoscale Visualization and Control of Ferroelectric Domains by Atomic-Force Microscopy. *Physical Review Letters.* **74** (21), 4309-4312 (1995).
15. Nikiforov, M.P., Thompson, G.L., Reukov, V.V., Jesse, S., Guo, S., Rodriguez, B.J., Seal, K., Vertegel, A.A., & Kalinin, S.V. Double-Layer Mediated Electromechanical Response of Amyloid Fibrils in Liquid Environment. *Acs Nano.* **4** (2), 689-698 (2010).
16. Botiz, I. & Darling, S.B. Optoelectronics using block copolymers. *Materials Today.* **13** (5), 42-51 (2010).
17. Brabec, C.J., Heeney, M., McCulloch, I., & Nelson, J. Influence of blend microstructure on bulk heterojunction organic photovoltaic performance. *Chemical Society Reviews.* **40** (3), 1185-1199 (2011).
18. Karagiannidis, P.G., Kassavetis, S., Pitsalidis, C., & Logothetidis, S. Thermal annealing effect on the nanomechanical properties and structure of P3HT: PCBM thin films. *Thin Solid Films.* **519** (12), 4105-4109 (2011).
19. Sweers, K., van der Werf, K., Bennink, M., & Subramaniam, V. Nanomechanical properties of alpha-synuclein amyloid fibrils: a comparative study by nanoindentation, harmonic force microscopy, and Peakforce QNM. *Nanoscale Research Letters.* **6**, (2011).
20. Nikiforov, M.P. & Darling, S.B. Improved conductive atomic force microscopy measurements on organic photovoltaic materials via mitigation of contact area uncertainty. *Progress in Photovoltaics: Research and Applications.*, doi:10.1002/pip.2217 (2012).
21. Li, H.-C., Rao, K.K., Jeng, J.-Y., Hsiao, Y.-J., Guo, T.-F., Jeng, Y.-R., & Wen, T.-C. Nano-scale mechanical properties of polymer/fullerene bulk hetero-junction films and their influence on photovoltaic cells. *Solar Energy Materials and Solar Cells.* **95** (11), 2976-2980 (2011).
22. Mueller, C., Goffri, S., Breiby, D.W., Andreasen, J.W., Chanzy, H.D., Janssen, R.A.J., Nielsen, M.M., Radano, C.P., Sirringhaus, H., Smith, P., & Stingelin-Stutzmann, N. Tough, semiconducting polyethylene-poly(3-hexylthiophene) diblock copolymers. *Advanced Functional Materials.* **17** (15), 2674-2679 (2007).
23. Kuila, B.K. & Nandi, A.K. Physical, mechanical, and conductivity properties of poly(3-hexylthiophene)-montmorillonite clay nanocomposites produced by the solvent casting method. *Macromolecules.* **37** (23), 8577-8584 (2004).
24. O'Connor, B., Chan, E.P., Chan, C., Conrad, B.R., Richter, L.J., Kline, R.J., Heeney, M., McCulloch, I., Soles, C.L., & DeLongchamp, D.M. Correlations between Mechanical and Electrical Properties of Polythiophenes. *Acs Nano.* **4** (12), 7538-7544 (2010).
25. Tahk, D., Lee, H.H., & Khang, D.-Y. Elastic Moduli of Organic Electronic Materials by the Buckling Method. *Macromolecules.* **42** (18), 7079-7083 (2009).
26. Kuila, B.K. & Nandi, A.K. Structural hierarchy in melt-processed poly(3-hexyl thiophene)-montmorillonite clay nanocomposites: Novel physical, mechanical, optical, and conductivity properties. *Journal of Physical Chemistry B.* **110** (4), 1621-1631 (2006).
27. Nikiforov, M.P. & Darling, S.B. Improved conductive atomic force microscopy measurements on organic photovoltaic materials via mitigation of contact area uncertainty. *Progress in Photovoltaics: Research and Applications.*, In Press, doi:10.1002/pip.2217 (2012).

28. Kim, J.Y., & Frisbie, D. Correlation of Phase Behavior and Charge Transport in Conjugated Polymer/Fullerene Blends. *Journal of Physical Chemistry C.* **112** (45), 17726-17736 (2008).
29. Bange, S., Kuksov, A., Neher, D., Vollmer, A., Koch, N., Ludemann, A., & Heun, S. The role of poly(3,4-ethylenedioxythiophene):poly(styrenesulphonate) as a hole injection layer in a blue-emitting polymer light-emitting diode. *Journal of Applied Physics.* **104** (10), (2008).